High resolution ZrF4-fiber-delivered multi-species infrared spectroscopy

Research Article Vol. 3, No. 12 / 15 December 2020 / OSA Continuum 3595

High resolution ZrF_4-fiber-delivered multi-species infrared spectroscopy

KERR JOHNSON,[1] PABLO CASTRO-MARIN,[2] OGUZHAN KARA,[2,3] CARL FARRELL,[1] AND DERRYCK T. REID[2,*]

[1]*Chromacity Ltd., Livingstone House, 43 Discovery Terrace, Research Avenue North, Riccarton, Edinburgh, EH14 4AP, United Kingdom*
[2]*Scottish Universities Physics Alliance (SUPA), Institute of Photonics and Quantum Sciences, School of Engineering and Physical Sciences, Heriot–Watt University, Edinburgh EH14 4AS, United Kingdom*
[3]*Leibniz Institute of Photonic Technology, Albert-Einstein srt. 9, Jena 07745, Germany*
[*]*d.t.reid@hw.ac.uk*

Abstract: Using coherent broadband mid-infrared light from a picosecond optical parametric oscillator we introduce a flexible, easy to use, high-resolution technique which can be utilized to conduct remote stand-off, or fiber delivered, multi-species spectroscopy in a spectroscopically cluttered environment. In particular, both narrow line-like and broad continuum-like species can be handled simultaneously. If only species with narrow line-like absorptions are present, this can be done without the need for an explicit reference spectrum. We demonstrate the approach by performing absorption spectroscopy of H_2O, CH_4, CH_3OH and C_2H_7NO (MEA) at high optical resolution (≈0.033 cm^{-1}) and via fiber delivery, opening the possibility of conducting multi-species spectroscopy in remote and hazardous environments. Spectral co-fitting of all absorption features and of the spectrum of the light-source provides a robust means of determining species concentrations, with detection limits of 290 ppb and 890 ppb obtained for CH_4 and MEA respectively using a 10.5-m Herriott cell and 32 seconds measurement time.

1. Introduction

Multi-species mid-infrared spectroscopy using active illumination [1] has widespread applications in combustion science [2–4], atmospheric pollution monitoring [5,6], breath analysis [7], process control [8–10], and chemical reaction monitoring [11]. Many of these applications require or would benefit from remote delivery, whether by using an open-path beam for atmospheric sensing over path lengths up to km [6,12], diffuse reflectance stand-off spectroscopy for chemical detection [13], or fiber delivery to an otherwise inaccessible environment. Recent approaches employed multiple quantum-cascade lasers (QCLs) or inter-band cascade lasers (ICLs) exhibiting significant tunability [14,15], or laser frequency combs based on optical parametric oscillators [16–20] or difference-frequency generation (DFG) [21]. These methods can access moderate to very high spectral resolutions (0.001–0.1 cm^{-1}), which are required when recording the narrow, line-like features of light molecules in the gas phase. However, techniques such as dual-comb spectroscopy [17–19] involve complex implementations, while multi-species spectroscopy of mixed gases presents specific challenges to established methods like tunable diode-laser spectroscopy, particularly where the species exhibit a mixture of line-like and continuum-like absorption features. For example, wavelength modulation spectroscopy with tunable distributed feedback (DFB) mid-infrared lasers was used to detect CO, CO_2, CH_4 and H_2O at elevated pressures in mixtures of synthesis gas [8], but doing so required careful identification of strong and sharp absorption features in an environment of highly blended lines. The presence of species with broad absorptions would make this much more challenging still. This example illustrates a

#412207 https://doi.org/10.1364/OSAC.412207
Journal © 2020 Received 12 Oct 2020; revised 26 Nov 2020; accepted 3 Dec 2020; published 14 Dec 2020

OSA CONTINUUM

common problem facing real-world multi-species spectroscopy, which is often complicated by the impracticality of acquiring a suitable reference measurement or otherwise implementing a reliable form of baseline correction when no absorption-free baseline exists. When the measurement must be made in an inaccessible or hazardous environment (e.g. a reaction vessel, combustion engine or petrochemical pipeline), the need to remotely deliver the spectroscopy light can further limit the opportunity for acquiring an independent reference measurement.

In this paper we introduce a flexible, easy to use high-resolution technique for conducting remote, multi-species spectroscopy in a spectroscopically cluttered environment. We demonstrate this for fiber delivery of mid-IR light to a gas cell, allowing simultaneous ro-vibrational spectroscopy of water, methane, methanol and monoethanolamine (MEA). Methanol and MEA are examples of species of interest in the context of air quality monitoring within enclosed environments.

2. Experimental methods

2.1. Optical parametric oscillator light source

All spectroscopy was performed using a commercial ultrafast optical parametric oscillator (Chromacity Ltd. OPO) similar to that reported elsewhere [6], producing idler pulses at a 300-MHz repetition rate, which were continuously tunable from 2.45–4.0 μm and had average powers of up to 400 mW. Example broadband spectra and corresponding average powers produced by the OPO across its tuning range are shown in Fig. 1.

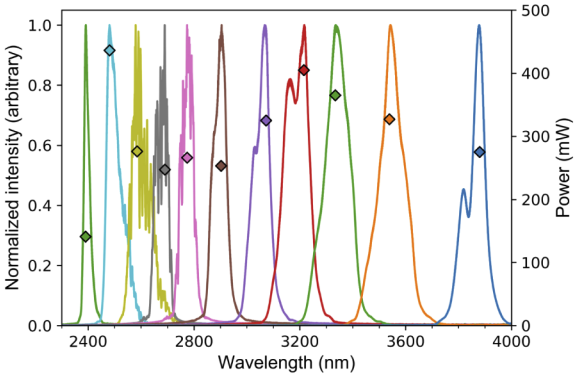

Fig. 1. OPO idler spectra and average powers.

2.2. Fourier-transform spectrometer

Figure 2 outlines the optical arrangement in which light from the OPO, typically covering wavelengths from 3.25–3.55 μm, was first coupled into a scanning Michelson interferometer before being launched into a 1m ZrF_4 single-mode delivery fiber with around 50% efficiency. This commercial fiber from Thorlabs (P1-23Z-FC-1) demonstrates the principle of fiber delivery and, depending on the application, can be substituted with longer lengths of similar fiber or bespoke hollow-core fibers designed for low-loss in the mid-IR [22,23]. Such hollow-core fibers can be drawn in >100m lengths so promise truly long-range delivery and will open the application space for this spectroscopy technique considerably. The fiber delivered the light into a 10.5-meter-long Herriott cell (Thorlabs HC10L/M-M02) supplied with re-circulating ambient air, optionally seeded with methanol and / or MEA. A thermoelectrically-cooled InAsSb amplified detector (Thorlabs PDA10PT-EC) was used to record a mid-IR interferogram of the transmitted light as the path difference of the Michelson interferometer was scanned at 1 Hz over a range of around 30 cm, corresponding to a spectroscopic resolution of 0.033 cm^{-1}. Individual

OSA CONTINUUM

interferograms were recorded with a measurement time of 500 ms every 19 s. Calibration fringes from a HeNe laser were recorded on a silicon detector. This configuration is based on previous free-space spectroscopic detection of hydrocarbons using mid-infrared OPO illumination, which achieved simultaneous concentration measurements of the mainly line-like spectra of H_2O, CH_4 and C_2H_6 at 0.05-cm^{-1} resolution and 100-ppb sensitivity [6]. Averaging improves the signal to noise ratio of the measurement, and typically 64 interferograms were recorded by the detector, with each being subsequently calibrated, Fourier-transformed and the resulting spectrum averaged with the others to produce the transmission spectra shown in Figs. 3–5. For species fully contained in the gas cell (methanol and MEA) the optical interaction length was 10.5 m, but an additional 3 m of open path between the OPO crystal and the gas cell increased the absorption from methane and water, which are present at atmospheric concentrations of 1.7–2.0 ppm and 0.5–1.0%, respectively.

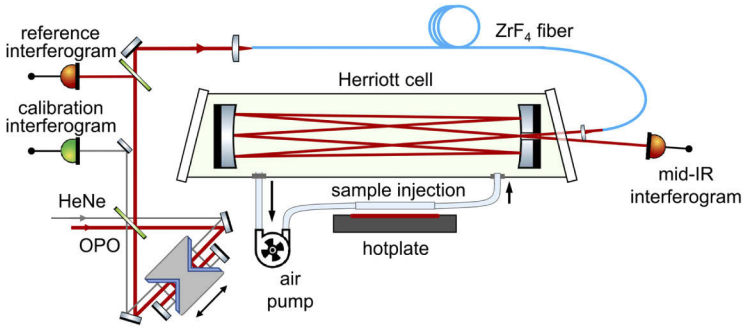

Fig. 2. OPO spectrometer and gas cell. Light from the OPO is routed through a scanning Michelson interferometer before being coupled into the delivery fiber. Calibration fringes from a HeNe laser are recorded in synchronism with the mid-IR interferogram and a reference interferogram recorded before the fiber.

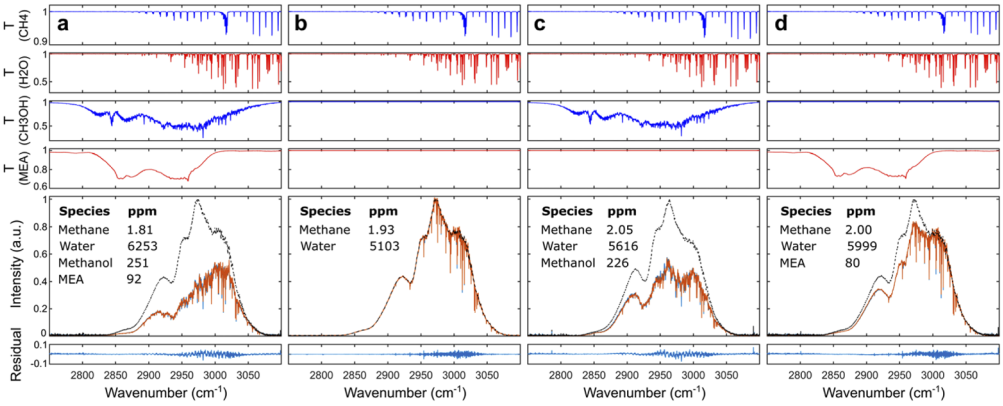

Fig. 3. (a) Average of 64 spectra acquired from a gas cell containing MEA and methanol (red), compared to the best-fit reference spectrum (blue) for MEA, methanol, water and methane. The co-fitted illumination envelope is shown by the dashed line. The fitted contributions from each chemical species are plotted as transmission spectra above the main plot. The residual is shown below, with most of the variance due to small line-shape fitting errors. (b)–(d) Equivalent fitting results for separate gas-cell experiments containing (b) only air, (c) air and methanol, and (d) air and MEA.

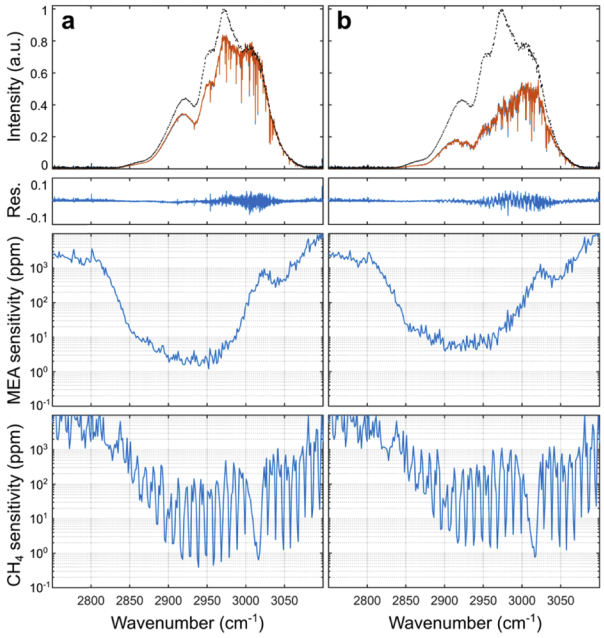

Fig. 4. Top row: simultaneous fit to methane, water vapor and (a) MEA, (b) MEA and methanol, showing the recorded transmission spectrum (red), the fitted spectrum (blue) and the recovered illumination spectrum (dashed). Second row: residuals between each fit and the corresponding measurement. Bottom two rows: Inferred sensitivity in ppm, with its variation across the spectrum, for MEA and methane. For CH_4 the strongest absorption only occurs local to the CH_4 absorption lines, meaning that the wavelength-dependent sensitivity resembles the line structure of the CH_4 absorption spectrum.

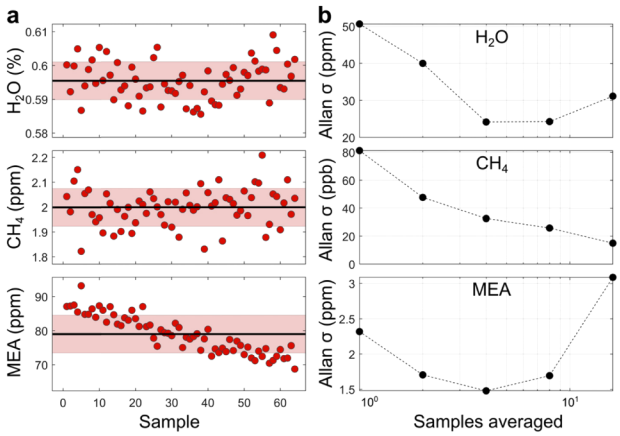

Fig. 5. (a) Concentrations recovered from 64 single-spectra simultaneous fits to methane, MEA and water vapor. The red region shows ± 1 standard deviation. (b) Allan deviations in concentration for averaging up to 16 samples.

OSA CONTINUUM

2.3. Sample preparation

The gas cell was connected to a closed-loop gas delivery system, illustrated in Fig. 2, consisting of a sample insertion tube and air pump. The sample vessel and gas cell were heated to 80°C using a hotplate and were insulated within an enclosure (not shown), allowing a significant fraction of MEA (which has low vapor pressure) to be maintained in the vapor phase. Air in the gas cell already contains water and methane at ambient concentrations, and both MEA and methanol were introduced by pipetting a small quantity of each (0.5 µl of methanol; 1 µl of MEA) into the gas recirculation loop while heating the gas cell. These quantities allowed us to infer maximum average concentrations of approximately 300 ppm for methanol and 400 ppm for MEA, but evaporation losses during pipetting and condensation at points within the gas circuit make these upper bounds only, rather than direct indicators of the expected concentration.

2.4. Spectral fitting procedure

Transmission spectra obtained directly from the apparatus described above were processed to remove étalon artefacts (by filtering out prominent peaks in Fourier space before applying an inverse Fourier transform to retrieve the spectra) and were then fitted to spectra from the HITRAN database [24,25] (water, methane and methanol), and proprietary absorbance data (MEA) in order to obtain the concentrations in the gas cell. As the gas cell was heated to 80°C all the reference spectra were appropriately scaled using the ideal gas law, and for the line-by-line calculated water and methane references the temperature (so line-broadening and partition function) was taken into account when retrieving the spectra [25]. The methanol reference spectrum was not calculated line-by-line so temperature effects on the line structure could not be accounted for. For species with sharp line-like absorption features, such as all the light molecules typically found in the atmosphere, the fitting algorithm can extract species concentrations and the spectral envelope without the need for a reference spectrum. Detailed elsewhere [6], the fitting algorithm first estimates the gas concentrations from an initial fit implemented by dividing the spectrum into many 5-cm^{-1} fragments, each of which is fitted by the absorbance coefficients of each of the gases and a two-point linear model of the local illumination envelope. This rapid process provides a robust starting point for a global optimization that refines the gas concentration values using the entire broadband spectrum, in which the illumination spectrum is modelled as a many-point spline function and is co-optimized with the concentrations of all the participating gas species. This procedure provides considerable benefits: for quantification when only line-like absorbers are present it implements baseline correction without the need for a reference spectrum; it naturally accommodates any absorption profile; it provides the best possible fit across the entire bandwidth of the spectrum; and it is fundamentally compatible with multi-species spectroscopy, requiring only one more fitting parameter per additional species. We note that this approach is particularly useful for atmospheric monitoring where it is not possible to take a baseline reference spectrum without the presence of the species of interest. While this approach can also be applied in the presence of heavier molecules with predominantly broad, slowly varying absorption features, the spline used to fit the spectral envelope may compete with the broad absorptions, reducing accuracy. Therefore, for improved accuracy in the case where there are species with broad absorption features, a reference detector simultaneously monitoring a fraction of the beam is picked off before delivery of light into the optical fiber. The ratio of this to the freely fitted envelope in the case of a cell filled with ambient air only (i.e. only line-like water and methane absorptions) constitutes a transfer function that can retrieve the spectral envelope, accounting for the systematic deviation caused by passage through the cell windows and optical fiber. For subsequent measurements in the presence of additional chemical species, the spectral envelope can be directly inferred by multiplying the reference detector spectrum by the transfer function.

OSA CONTINUUM

3. Results and discussion

3.1. Spectroscopy and spectral fitting

The ambient concentrations of water vapor and methane, together with those of methanol and MEA provide a complex spectral landscape, with most regions of the spectrum experiencing strong attenuation, and with comparable maximum cross-sections for all four species. Water vapor and methane contribute predominantly line-like absorptions, methanol a broad continuum with many superimposed narrow absorption features, and MEA a relatively smooth and slowly varying profile. Methanol was chosen because the molecule is not so small and simple that it has only widely spaced C-H line-like absorptions, yet not so large that the C-H absorptions form a smooth continuum. It therefore provides a challenging test of multi-species spectroscopy for both line-like and broadly absorbing species. Figure 3(a) shows an example of the resultant fitting to the average of 64 spectra from a gas cell containing methanol and MEA. The best fit of the MEA, methanol, water and methane reference data is compared to the experimental spectrum. The co-fitted illumination envelope is shown by the dashed line. The fitted contributions from each chemical species are plotted as transmission spectra in the upper panels while the residual of the fit is shown below. These residuals occur due to small line-shape errors which are expected due to the sensitivity of the actual data to temperature and pressure variations that may not be accounted for in the reference spectra. The concentrations returned are consistent with the values expected for water and methane abundances in atmospheric air (here around 0.5–1.0% water and 1.7–2.0 ppm methane, although as these are indoor measurements there are additional sources and sinks meaning the values can vary considerably), while those of methanol and MEA are within the upper bounds set by the total volume of each chemical introduced into the system.

Figures 3(b)–3(d) show the equivalent fitting results for separate gas cell experiments containing (b) air, (c) air and methanol, and (d) air and MEA. The contributions of the species present can be well fitted and their concentrations extracted. The mainly line-like absorption of methane and water means that the illumination envelope is clearly evident in Fig. 3(b), modulated only by the narrow absorption lines of the two gases. In this case the envelope was fitted without the use of the reference detector and clearly indicates that reference-free spectroscopy can be implemented in situations where there are only narrow line-like absorptions, such as atmospheric monitoring. For panels (a), (c) and (d), the transfer function calculated from the data in (b) was used in conjunction with the spectrum recorded on the reference detector to determine the envelope of the OPO light. This illumination envelope varies by a small amount from measurement to measurement (separated by hours) due to slow and small environmental changes manifesting themselves in the OPO spectral structure.

3.2. Detection sensitivity analysis

The data presented in Fig. 3 can be used to determine the minimum sensitivity for the detection of any given species. As an example we consider here the detection of MEA and methane, and the impact of the spectrally interfering methanol. The Beer-Lambert law provides the transmitted intensity as $I = I_o e^{-\alpha\chi L}$, where I_o is the source intensity, α is the absorbance in ppm^{-1} m^{-1}, χ is the concentration in ppm and L is the cell length in meters. Differentiating gives $\Delta\chi = -\Delta I/\alpha L I$, which is the minimum concentration change that can be detected over the noise (one standard deviation) in the intensity spectrum, ΔI.

We applied this analysis to establish the detection sensitivity for MEA and methane in air (Fig. 4(a)), and in the presence of methanol (Fig. 4(b)), which spectrally interferes with methane and MEA. Each spectrum in Fig. 4 is obtained from the average of 64 spectra, which increases the signal to noise by a factor of eight, compared with a single acquisition. The sensitivity plots in Fig. 4 were obtained by analyzing the data in small (approximately 1.5 cm^{-1}) sections, and for

OSA CONTINUUM

each of these calculating $\Delta\chi$ using the appropriate source intensity, the standard deviation of the residual of the fit as ΔI, and the maximum value of α for MEA/CH_4 within the section.

For the results in Fig. 4(a), (a) sensitivity of 1.2 ppm is observed for MEA around 2952 cm^{-1}, a region where MEA has a high value of α, the source intensity is strong ($I \approx 0.72 I_o$) and the water absorption is relatively weak. In the low concentration limit ($I \approx I_o$) this result implies a detection limit, or minimum detectable concentration, of 890 ppb (9.3 ppm·m), approaching the continuous exposure guidance level for MEA of 500 ppb [26]. Equivalent analysis for methane results in a sensitivity of 400 ppb, with a detection limit of 290 ppb (3.9 ppm·m). A similar analysis for the dataset from the gas cell containing both methanol and MEA (Fig. 4(b)) yields a sensitivity of 4 ppm for MEA and 0.8 ppm for methane, corresponding to 1.44 ppm and 475 ppb in the low-concentration detection limit. Methanol contains many closely spaced yet sharp absorption features which overlap the MEA spectrum considerably and make the fitting more challenging. In addition, as the line shapes in the methanol reference spectrum used could not be corrected for temperature this will also contribute to an increase in noise and so reduction in sensitivity of MEA detection in the presence of methanol. The analysis indicates that the absolute sensitivity is impacted by strong spectral interference from other species, but not to an overwhelming degree. We note that the sensitivity plots presented here are calculated on a point-by-point basis from the local noise on the residual of the fit and the local absorption cross section. If the sensitivity were calculated globally, one can expect a further 'multi-line fitting' improvement in the sensitivity as explored in [20], in which for example, an 11-fold improvement in methane sensitivity is predicted.

The methane sensitivity of 3.9 ppm·m reported here is comparable with other remote FTIR spectroscopy techniques and commercial systems [6,12,27], which achieve 1–4 ppm·m sensitivity. It also approaches sensitivities achieved using frequency comb implementations, for example the reported detection sensitivities for acetone and isopropanol of 5.7 ppm·m and 2.4 ppm·m respectively, [12]. Broadband mid-infrared resonant cavity techniques have achieved multi-species detection with absolute sensitivities of around 2 ppb [28], but at the expense of a more complex experimental arrangement.

3.3. Spectral averaging and measurement precision

An Allan deviation analysis allows us to assess the impact of averaging on the precision of the concentration measurement we obtain when there is a fluctuation in the parameters of the measurement e.g. variability in the concentration of the gas, or instability of the measurement system. The results described so far utilized an average of 64 spectra to produce a single low-noise spectrum, which was then subjected to the spectral fitting procedure. However, spectral fitting can also be readily performed on individual spectra to obtain concentration values from a single measurement. We conducted independent three-species fits (CH_4, H_2O and MEA) to 64 spectra obtained over the course of 20 minutes, where each spectrum was generated from a single interferogram acquired every 19 seconds in a time of 500 ms. The Allan deviation analysis of the resulting concentration values is presented in Fig. 5 and shows different behaviors for the CH_4, H_2O and MEA measurements. The Allan deviation for CH_4, whose ambient concentration is subject to only minimal systematic variation, continues to improve with more samples, reaching a precision of 20 ppb after 16 samples (5 minutes' acquisition time). Conversely, both H_2O and MEA display a systematic trend (Fig. 5(b)), limiting the useful averaging time to ~75-seconds (four samples) over which the concentration is approximately stable. These systematic trends imply instabilities in the actual concentrations of H_2O and MEA over longer timescales, both of which are most likely due to a temperature drift of the gas-cell enclosure affecting the proportions of H_2O and MEA in the vapor phase.

If the data acquisition, processing, and storage were to be optimized, the time per spectrum (including all overheads) would more closely approach the actual 500 ms of stage movement

OSA CONTINUUM

time required to record the interferogram. In this case the optimum precision would improve as more samples could be averaged before the Allan deviation reached a minimum. Similar experimental arrangements [6] have been optimized to acquire at three seconds per spectra. We therefore note that the precisions inferred from these Allan deviation data are specific to this particular experimental configuration and could be significantly improved by faster acquisition techniques. By extracting concentration data from fits to individual spectra, faster acquisition would also enable real-time concentration monitoring in situations where one is not operating near the detection limit.

4. Conclusions

The results presented here demonstrate the practicality of fiber-delivered multi-species spectroscopy in a spectroscopically cluttered environment, and are enabled by a number of factors. The use of a coherent mid-infrared light source provides a high quality, high brightness beam that remains well overlapped over the considerable scan range of a high resolution Fourier-transform Michelson interferometer, is compatible with fiber delivery and can subsequently be efficiently coupled into a long multi-pass gas cell. The broad bandwidth enables reliable multi-species spectral fitting to ground-truth reference absorbance data, and concentrations to be confidently extracted using a global spectral fitting algorithm. We have shown the procedure to be robust in the presence of spectrally interfering species that exhibit both line-like and continuum-like absorption features, even where these occur with a periodicity similar to variations in the illumination spectrum. By applying a noise-equivalent absorption analysis we have shown how the detection sensitivity of an individual species can be inferred from the complete multi-species dataset, which can allow regions to be identified in which there is high sensitivity to one species, while high tolerance to fluctuations in another. When the concentration of the species being measured is stable, averaging provides the expected improvement in measurement precision, and the presence of systematic variations can be inferred independently for each species from the full multi-species dataset. Finally, while this study has concerned only species in the vapor phase, the technique is also well suited to situations involving detection and quantification of liquids and solids, a scenario in which the broad bandwidth is crucial as there are generally no narrow absorption features. The approach described here therefore opens the way to versatile, fiber-delivered remote spectroscopy of chemical mixtures, requiring only a simple photodetector located at the distal end of the fiber.

Funding

Defence and Security Accelerator (ACC2006559); Engineering and Physical Sciences Research Council (EP/P030181/1); Science and Technology Facilities Council (ST/T000635/1).

Disclosures

CF: Chromacity Ltd. (I,E); KJ: Chromacity Ltd. (E); DTR: Chromacity Ltd. (I); PCM and OK declare no conflicts of interest.

References

1. K. C. Cossel, E. M. Waxman, I. A. Finneran, G. A. Blake, J. Ye, and N. R. Newbury, "Gas-phase broadband spectroscopy using active sources: progress, status, and applications [Invited]," J. Opt. Soc. Am. B **34**(1), 104 (2017).
2. A. Kosterev, G. Wysocki, Y. Bakhirkin, S. So, R. Lewicki, M. Fraser, F. Tittel, and R. F. Curl, "Application of quantum cascade lasers to trace gas analysis," Appl. Phys. B **90**(2), 165–176 (2008).
3. Zeng Hui, D. Ou, and G. Kang, "Multispecies combustion diagnostics using tunable diode laser absorption spectroscopy," in *Fifth International Symposium on Laser Interaction with Matter*, Y. Zhao, ed. (SPIE, 2019).
4. C. A. Alrahman, A. Khodabakhsh, F. M. Schmidt, Z. Qu, and A. Foltynowicz, "Cavity-enhanced optical frequency comb spectroscopy of high-temperature H_2O in a flame," Opt. Express **22**(11), 13889 (2014).

OSA CONTINUUM

5. M. Rutkauskas, M. Asenov, S. Ramamoorthy, and D. T. Reid, "Autonomous multi-species environmental gas sensing using drone-based Fourier-transform infrared spectroscopy," Opt. Express **27**(7), 9578 (2019).
6. O. Kara, F. Sweeney, M. Rutkauskas, C. Farrell, C. G. Leburn, and D. T. Reid, "Open-path multi-species remote sensing with a broadband optical parametric oscillator," Opt. Express **27**(15), 21358 (2019).
7. M. J. Thorpe, D. Balslev-Clausen, M. S. Kirchner, and J. Ye, "Cavity-enhanced optical frequency comb spectroscopy: application to human breath analysis," Opt. Express **16**(4), 2387 (2008).
8. R. Sur, K. Sun, J. B. Jeffries, and R. K. Hanson, "Multi-species laser absorption sensors for in situ monitoring of syngas composition," Appl. Phys. B **115**(1), 9–24 (2014).
9. K. Eslami Jahromi, Q. Pan, A. Khodabakhsh, C. Sikkens, P. Assman, S. M. Cristescu, P. M. Moselund, M. Janssens, B. E. Verlinden, and F. J. M. Harren, "A Broadband Mid-Infrared Trace Gas Sensor Using Supercontinuum Light Source: Applications for Real-Time Quality Control for Fruit Storage," Sensors **19**(10), 2334 (2019).
10. N. Lang, A. D. F. Puth, S. Klose, G. Kowzan, S. Hamman, J. Röpcke, P. Maslowski, and J. H. van Helden, "Direct Mid-Infrared Frequency Comb Spectroscopy of Nitrocarburizing Plasma Processes," in *Light, Energy and the Environment 2018 (E2, FTS, HISE, SOLAR, SSL), OSA Technical Digest* (Optical Society of America, 2018), paper FM2B.6.
11. B. J. Bjork, T. Q. Bui, O. H. Heckl, P. B. Changala, B. Spaun, P. Heu, D. Follman, C. Deutsch, G. D. Cole, M. Aspelmeyer, M. Okumura, and J. Ye, "Direct frequency comb measurement of OD + CO -> DOCO kinetics," Science **354**(6311), 444–448 (2016).
12. G. Ycas, F. R. Giorgetta, K. C. Cossel, E. M. Waxman, E. Baumann, N. R. Newbury, and I. Coddington, "Mid-infrared dual-comb spectroscopy of volatile organic compounds across long open-air paths," Optica **6**(2), 165 (2019).
13. Z. Zhang, R. J. Clewes, C. R. Howle, and D. T. Reid, "Active FTIR-based stand-off spectroscopy using a femtosecond optical parametric oscillator," Opt. Lett. **39**(20), 6005 (2014).
14. S. O'Hagan, J. H. Northern, B. Gras, P. Ewart, C. S. Kim, M. Kim, C. D. Merritt, W. W. Bewley, C. L. Canedy, I. Vurgaftman, and J. R. Meyer, "Multi-species sensing using multi-mode absorption spectroscopy with mid-infrared interband cascade lasers," Appl. Phys. B **122**(6), 173 (2016).
15. G. Wysocki, R. Lewicki, R. F. Curl, F. K. Tittel, L. Diehl, F. Capasso, M. Troccoli, G. Hofler, D. Bour, S. Corzine, R. Maulini, M. Giovannini, and J. Faist, "Widely tunable mode-hop free external cavity quantum cascade lasers for high resolution spectroscopy and chemical sensing," Appl. Phys. B **92**(3), 305–311 (2008).
16. L. Maidment, P. G. Schunemann, and D. T. Reid, "Molecular fingerprint-region spectroscopy from 5 to 12 μm using an orientation-patterned gallium phosphide optical parametric oscillator," Opt. Lett. **41**(18), 4261 (2016).
17. Z. Zhang, T. Gardiner, and D. T. Reid, "Mid-infrared dual-comb spectroscopy with an optical parametric oscillator," Opt. Lett. **38**(16), 3148 (2013).
18. O. Kara, L. Maidment, T. Gardiner, P. G. Schunemann, and D. T. Reid, "Dual-comb spectroscopy in the spectral fingerprint region using OPGaP optical parametric oscillators," Opt. Express **25**(26), 32713 (2017).
19. A. V. Muraviev, V. O. Smolski, Z. E. Loparo, and K. L. Vodopyanov, "Massively parallel sensing of trace molecules and their isotopologues with broadband subharmonic mid-infrared frequency combs," Nat. Photonics **12**(4), 209–214 (2018).
20. F. Adler, P. Masłowski, A. Foltynowicz, K. C. Cossel, T. C. Briles, I. Hartl, and J. Ye, "Mid-infrared Fourier transform spectroscopy with a broadband frequency comb," Opt. Express **18**(21), 21861 (2010).
21. H. Timmers, A. Kowligy, A. Lind, F. C. Cruz, N. Nader, M. Silfies, G. Ycas, T. K. Allison, P. G. Schunemann, S. B. Papp, and S. A. Diddams, "Molecular fingerprinting with bright, broadband infrared frequency combs," Optica **5**(6), 727 (2018).
22. N. V. Wheeler, A. M. Heidt, N. K. Baddela, E. N. Fokoua, J. R. Hayes, S. R. Sandoghchi, F. Poletti, M. N. Petrovich, and D. J. Richardson, "Low-loss and low-bend-sensitivity mid-infrared guidance in a hollow-core–photonic-bandgap fiber," Opt. Lett. **39**(2), 295 (2014).
23. F. Yu, W. J. Wadsworth, and J. C. Knight, "Low loss silica hollow core fibers for 3–4 μm spectral region," Opt. Express **20**(10), 11153 (2012).
24. I. E. Gordon, L. S. Rothman, C. Hill, R. V. Kochanov, Y. Tan, P. F. Bernath, M. Birk, V. Boudon, A. Campargue, K. V. Chance, B. J. Drouin, J.-M. Flaud, R. R. Gamache, J. T. Hodges, D. Jacquemart, V. I. Perevalov, A. Perrin, K. P. Shine, M.-A. H. Smith, J. Tennyson, G. C. Toon, H. Tran, V. G. Tyuterev, A. Barbe, A. G. Császár, V. M. Devi, T. Furtenbacher, J. J. Harrison, J.-M. Hartmann, A. Jolly, T. J. Johnson, T. Karman, I. Kleiner, A. A. Kyuberis, J. Loos, O. M. Lyulin, S. T. Massie, S. N. Mikhailenko, N. Moazzen-Ahmadi, H. S. P. Müller, O. V. Naumenko, A. V. Nikitin, O. L. Polyansky, M. Rey, M. Rotger, S. W. Sharpe, K. Sung, E. Starikova, S. A. Tashkun, J. V. Auwera, G. Wagner, J. Wilzewski, P. Wcisło, S. Yu, and E. J. Zak, "The HITRAN 2017 molecular spectroscopic database," J. Quant. Spectrosc. Radiat. Transfer **203**, 3–69 (2017).
25. R. V. Kochanov, I. E. Gordon, L. S. Rothman, P. Wcisło, C. Hill, and J. S. Wilzewski, "HITRAN Application Programming Interface (HAPI): A comprehensive approach to working with spectroscopic data," J. Quant. Spectrosc. Radiat. Transfer **177**, 15–30 (2016).
26. *Emergency and Continuous Exposure Guidance Levels for Selected Submarine Contaminants* (National Academies Press, 2007).
27. Bruker, D-fenceline™ and OPS, https://brukeropenpath.com/atmosfir-d-fenceline/.
28. A. J. Fleisher, B. J. Bjork, T. Q. Bui, K. C. Cossel, M. Okumura, and J. Ye, "Mid-Infrared Time-Resolved Frequency Comb Spectroscopy of Transient Free Radicals," J. Phys. Chem. Lett. **5**(13), 2241–2246 (2014).